Performance of Pre-Swirl Rotating-Disc Systems

Hasan Karabay
Robert Pilbrow[1]
Michael Wilson
J. Michael Owen

Department of Mechanical Engineering,
Faculty of Engineering and Design,
University of Bath,
Bath BA2 7AY, UK

This paper summarizes and extends recent theoretical, computational, and experimental research into the fluid mechanics, thermodynamics, and heat transfer characteristics of the so-called cover-plate pre-swirl system. Experiments were carried out in a purpose-built rotating-disc rig, and the Reynolds-averaged Navier-Stokes equations were solved using two-dimensional (axisymmetric) and three-dimensional computational codes, both of which incorporated low-Reynolds-number k-ε turbulence models. The free-vortex flow, which occurs inside the rotating cavity between the disc and cover-plate, is controlled principally by the pre-swirl ratio, β_p: this is the ratio of the tangential velocity of the air leaving the nozzles to that of the rotating disc. Computed values of the tangential velocity are in good agreement with measurements, and computed distributions of pressure are in close agreement with those predicted by a one-dimensional theoretical model. It is shown theoretically and computationally that there is a critical pre-swirl ratio, $\beta_{p,crit}$, for which the frictional moment on the rotating discs is zero, and there is an optimal pre-swirl ratio, $\beta_{p,opt}$, where the average Nusselt number is a minimum. Computations show that, for $\beta_p < \beta_{p,opt}$, the temperature of the blade-cooling air decreases as β_p increases; for $\beta_p > \beta_{p,opt}$, whether the temperature of the cooling air increases or decreases as β_p increases depends on the flow conditions and on the temperature difference between the disc and the air. Owing to the three-dimensional flow and heat transfer near the blade-cooling holes, and to unquantifiable uncertainties in the experimental measurements, there were significant differences between the computed and measured temperatures of the blade-cooling air. In the main, the three-dimensional computations produced smaller differences than the two-dimensional computations. [S0742-4795(00)01902-5]

1 Introduction

Pre-swirl nozzles are used in many gas turbines to supply the cooling air to the turbine blades. The stationary nozzles swirl the air in the direction of rotation of the turbine disc, thereby reducing the temperature of the air relative to the blades. In the so-called cover-plate pre-swirl system shown in Fig. 1, the pre-swirl nozzles are located at a radius $r=r_1$ and the entrance to the blade-cooling passages is at $r=r_2$, where $r_2>r_1$. The swirling air flows radially outwards in the rotating cavity between the rotor (or rotating disc) and a cover-plate attached to it.

Pre-swirl systems have been studied by many research workers, and the reader is referred to the work of Meierhofer and Franklin [1], El-Oun and Owen [2], Chen et al. [3,4], Popp et al. [5], Wilson et al. [6], Karabay et al. [7], and Pilbrow et al. [8]. Some of the authors' recent results for cover-plate pre-swirl systems are briefly reviewed below.

Karabay et al. [7] showed, computationally and experimentally, that the flow between the rotating cover-plate and the stator was like a conventional rotor-stator system, in which a disc rotates close to a stationary casing (see Owen and Rogers [9]), and the flow between the cover-plate and the rotor was like that in a rotating cavity in which two discs corotate (see Owen and Rogers [10]). In particular, at the high coolant flow rates that occur in practical cases, free-vortex flow occurs outside the boundary layers in the rotating cavity. Pilbrow et al. [8] extended this work to include heat transfer from the rotor to the cooling air, and computations of the local Nusselt numbers were in reasonably good agreement with measured values for a wide range of pre-swirl ratios, β_p, nondimensional coolant flow rates, C_w, and rotational Reynolds numbers, Re_ϕ.

Karabay et al. [11] conducted a combined theoretical and computational study of the flow and heat transfer in the ''simple ro-

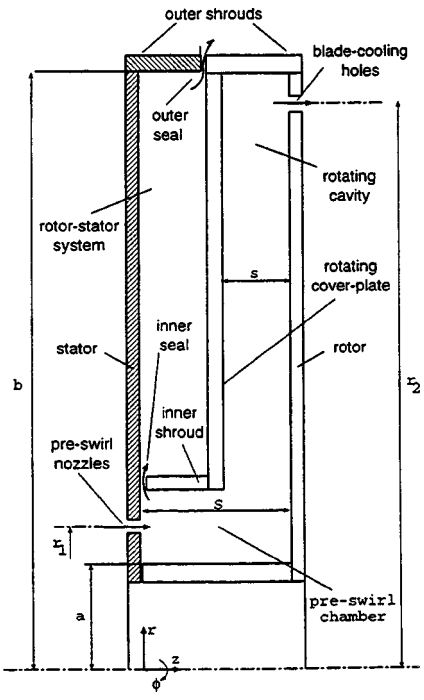

Fig. 1 Simplified diagram of cover-plate pre-swirl system (for the rig used in this study: $a=80$ mm, $b=207$ mm, $r_1=90$ mm, $r_2=200$ mm, $S=25$ mm, $s=10$ mm)

[1]Now at Rolls Royce plc, Bristol, UK.

Contributed by the International Gas Turbine Institute (IGTI) of THE AMERICAN SOCIETY OF MECHANICAL ENGINEERS for publication in the ASME JOURNAL OF ENGINEERING FOR GAS TURBINES AND POWER. Paper presented at the International Gas Turbine and Aeroengine Congress and Exhibition, Indianapolis, IN, June 7–10, 1999; ASME Paper 99-GT-197. Manuscript received by IGTI March 9, 1999; final revision received by the ASME Headquarters January 3, 2000. Associate Technical Editor: D. Wisler.

tating cavity,'' disregarding the rest of the cover-plate system. They derived an expression for the radial distribution of pressure, and used the Reynolds analogy to derive a relationship for the adiabatic-disc temperature. For the case where there is free-vortex flow throughout the rotating cavity, there is a critical pre-swirl ratio, $\beta_{p,\mathrm{crit}}$, for which the moment coefficient, C_m, is zero, and an optimal pre-swirl ratio, $\beta_{p,\mathrm{opt}}$, for which the average Nusselt number of the heated rotor is a minimum. Karabay's [12] thesis is concerned with the computation of flow and heat transfer in pre-swirl systems, and this paper presents some of these computations.

It is the object of this paper to extend the previous work and to provide some guidance for the designers of internal cooling-air systems. In particular, the designer is interested in the pressure drop associated with pre-swirl systems and needs to know the effect of β_p on the temperature of the blade-cooling air when heat transfer from the turbine disc is significant. Previous computational work has concentrated on axisymmetric systems, but three-dimensional effects can be significant near the blade-cooling holes in the rotor, as discussed below.

Section 2 of the paper outlines the computational method and experimental apparatus used in this study. The fluid dynamics of the cover-plate system shown in Fig. 1 is discussed in Section 3, and the thermodynamics and heat transfer in Section 4. The conclusions are summarized in Section 5.

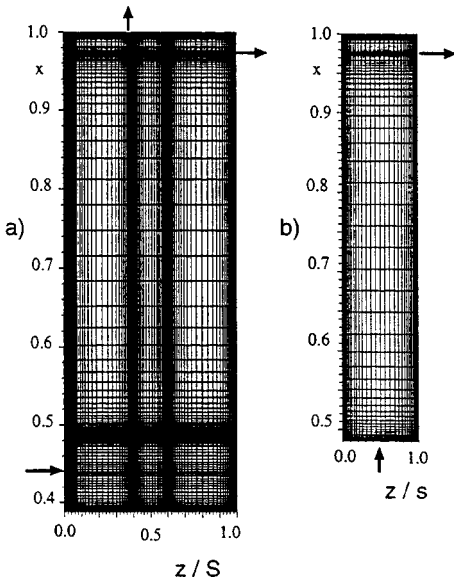

Fig. 2 Grid distributions used for computations: (*a*) whole system; (*b*) simple cavity.

2 Computational and Experimental Methods

2.1 Computational Model. The computational model has been described by Karabay et al. [7] and further details are given by Karabay [12]. For completeness, the salient points of the model are given below.

Turbulent flow computations were made using the low-Reynolds, number k-ε models of Launder-Sharma [13] and of Morse [14]. Both used gradient-diffusion modeling of transport, and the latter model incorporated modifications suggested by its author (see Chen et al. [15] for details). Incompressible flow was assumed and turbulent heat transfer was represented using a turbulent Prandtl number Pr_t equal to 0.9.

A staggered grid was used in which the axial and radial velocity components were stored midway between the grid-points where other solution variables were located (pressure, tangential velocity, turbulence kinetic energy and dissipation rate, and total enthalpy). The cover-plate and inner shroud (see Fig. 1) were represented by block obstructions within the computational grid and the equations were solved using the SIMPLEC pressure-correction algorithm.

The inlet nozzles and blade-cooling holes of the experimental rig were represented in the axisymmetric model by equivalent-area annular slots on the stator and rotor, with centerlines at $r=r_1$ and $r=r_2$, respectively. The axial velocity of the pre-swirl air, $V_{z,p}$, which was assumed to be uniform at the inlet, was deduced from the prescribed flow rate. Similarly, the axial velocity at the blade-cooling slot and the radial velocity at the outer seal were calculated from prescribed flow rates.

The inlet tangential velocity, $V_{\phi,p}$, was fixed to give the required pre-swirl ratio β_p, and Neumann (zero normal-derivative) boundary conditions for tangential velocity were used at the two outlets ($\partial V_\phi/\partial z=0$ at the blade-cooling slot and $\partial V_\phi/\partial r=0$ at the outer seal). The remaining velocity components at flow boundaries were taken to be zero, and no-slip conditions were applied at all solid surfaces. The inlet temperature of the pre-swirl air and the surface temperature distribution of the rotor (see Fig. 1) were taken from measured values (Karabay et al. [7]). The surfaces of the shrouds, the stator, the cover-plate and the inner casing at $r=a$ were all assumed adiabatic. At the blade-cooling slot, $\partial T/\partial z=0$ was assumed, and $\partial T/\partial r=0$ was used for the flow leaving at the outer seal.

The turbulence models required a very fine grid near the boundaries, with $y^+<0.5$ for the near-wall grid nodes, and the grid-spacing increased geometrically away from walls (including the cover-plate and shroud) with expansion factors of about 1.2. Computations were conducted for the ''whole system,'' corresponding to the complete cover-plate system shown in Fig. 1, and for the smaller ''simple cavity,'' corresponding to the rotating cavity between the rotor and the cover-plate shown in Fig. 1. Only two-dimensional (axisymmetric) computations were carried out in the ''whole system'' the ''simple cavity'' was used for the two-dimensional and three-dimensional computations described in Section 4.4. A 223 by 223 axial by radial grid was used for the ''whole system''; for the ''simple cavity'' a 67 by 111 axial by radial grid was used (see Fig. 2). (Computations were also conducted with a 141×185 grid, which made no significant difference to the comparison between the computed and measured Nusselt numbers; this suggests that the results presented below are sensibly grid-independent.)

2.2 Experimental Apparatus. A diagram of the rotating-disc rig is shown in Fig. 3, and details of the apparatus are given by Pilbrow et al. [8]. The main features of the apparatus are summarized below, and the total-temperature probes are described in detail. Although two pressure transducers were fitted to the cover-plate, an accident with the rig damaged the wiring and so it was not possible to obtain pressure measurements.

2.2.1 Rotating-Disc Rig. The outer radius of the system, b, was approximately 207 mm, and the radial locations of the pre-swirl nozzles and blade-cooling holes were $r_1=90$ mm and $r_2=200$ mm. There were 19 pre-swirl nozzles of 7.92 mm diameter, angled at 20 deg to the tangential direction, and 60 blade-cooling holes of 7.7 mm diameter, with their axes normal to the rotor. The pre-swirl nozzles were made from stainless-steel tubes, which were bent through an angle of 70 deg to produce the required swirl angle. The outlet ends of the tube were ground so that they were flush with the surface of the stator. The outlet holes from the pre-swirl nozzles were therefore elliptic when viewed from the axial direction. The axial spacing between the 5-mm-thick cover-plate and the stator was 10 mm, and between the cover-plate and the rotor the spacing was also 10 mm.

The rotor was of composite construction, comprising a steel front disc, two layers of Rohacell foam and an aluminum back disc. A 1-mm-thick fibre-glass mat was bonded to the front (cavity-side) face of the steel disc, which was 10-mm thick, and 10 thermocouples and 6 fluxmeters were embedded in the surface

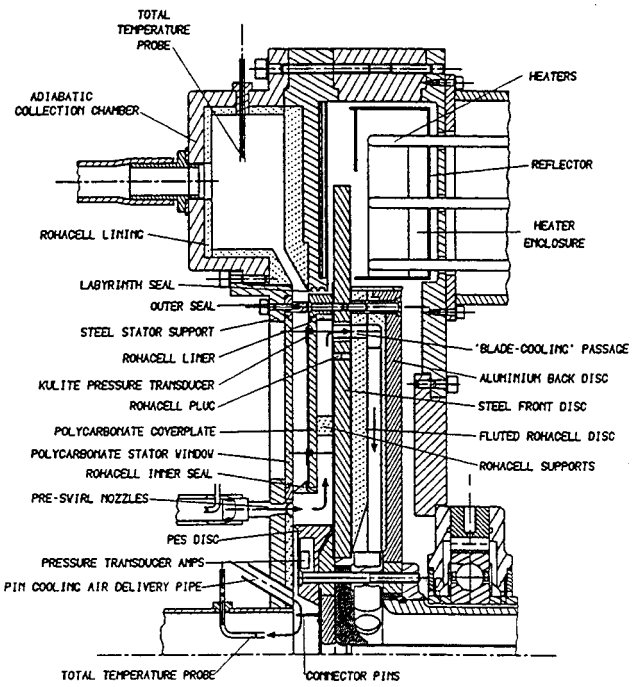

Fig. 3 Diagram of the rotating-disc rig

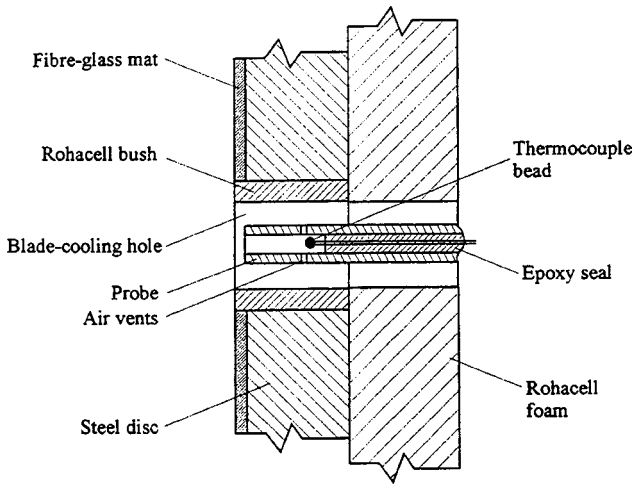

Fig. 4 Details of total-temperature probe located in blade-cooling hole (not to scale)

of the mat. The Rohacell foam provided thermal insulation, for the back of the steel disc, and contained passages for the blade-cooling air; each layer of foam was approximately 10-mm thick. The signals from all the rotating instrumentation were brought out through a 24-channel silver/silver graphite slipring unit, and the voltages were measured with a precision of ± 1 μV by a computer-controlled Solartron data logger.

The outer part of the rotating disc was heated up to 150°C by means of stationary radiant electric heater units, with a maximum power output of 9.5 kW. The actual temperature distribution over the instrumented section of the disc depended on the heat conducted radially inwards from the periphery. The maximum temperature in the instrumented section of the disc was around 70°C, but it depended on the rotational speed and on the flow rate of the cooling air. The temperature of the air at the pre-swirl nozzles was maintained at between 10°C and 20°C.

For a typical engine, $\mathrm{Re}_\phi \approx 10^7$, $\lambda_T \approx 0.3$, $\beta_p \approx 2.5$. For the heat transfer tests in the rig, the following range of parameters was tested: $0.5\times10^5 < \mathrm{Re}_\phi < 1.6\times10^6$, $0.16 < \lambda_T < 0.32$, $0.9 < \beta_p < 3.1$. It is shown in Section 3.1 that the flow structure depends principally on λ_T and β_p. The rig is therefore able to model the flow structures expected in engines, although the Nusselt numbers and temperatures measured in the rig are much smaller than those found in engines.

2.2.2 Total-Temperature Probes. The blade-cooling holes in the steel disc were insulated with Rohacell bushes, with inner and outer diameters of 7.7 and 12.0 mm. Two total-temperature probes, see Fig. 4, were placed in diametrically opposite blade-cooling holes with the tip of each probe set back about 0.5 mm from the disc face. To reduce the blockage effect of the probes, the inner diameter of the Rohacell bushes was increased for these two blade-cooling holes. The probes were made from stainless-steel tubes, with inner and outer diameters of 2.8 and 3.2 mm, and two air vents of 0.5 mm diameter were drilled radially through each tube, as shown. The thermocouple wires were 0.10 mm diameter, and the 0.2 mm diameter bead was located downstream of the vents. Behind the bead, the tube was sealed with epoxy resin.

There are two significant problems in designing a probe to measure the total-temperature of the blade-cooling air. First, it is not easy to create solid-body rotation in swirling air flowing through a short, rotating hole, the axis of which is parallel to the axis of rotation. Meierhofer and Franklin [1] pointed out the problems they experienced while measuring the blade-coolant temperature in an adiabatic system. However, the probe-design described above was used successfully by El-Oun and Owen [2] to measure the total temperature of the blade-cooling air in an unheated pre-swirl rig, similar to the heated version used here. They estimated the uncertainty in their temperature measurements as ± 0.3°C, and their measured values were in good agreement with the theoretical temperatures for an adiabatic system. This suggests that the experimental uncertainties in measurements made with the probe used here should be small in an *adiabatic system*.

The second problem in temperature measurement occurs when heat transfer from the disc to the cooling air is significant: the Rohacell bushes in the blade-cooling holes reduce but do not cure this problem. As described in Section 4, computations show that there are large gradients of air temperatures in and around the blade-cooling holes, and it is unlikely that the probe described above will measure the true bulk-average temperature of the blade-cooling air. The uncertainties cannot be quantified.

3 Fluid Dynamics

3.1 Flow structure. As shown by Owen and Rogers [10], the flow structure in a rotating cavity depends principally on the inlet swirl ratio and the turbulent flow parameter, λ_T, where $\lambda_T = C_W \mathrm{Re}_\phi^{-0.8}$. It is helpful to note that $\lambda_T = \lambda_{T,fd} = 0.22$ corresponds to the nondimensional flow rate entrained by the boundary layer on one surface of a free-disc. From the authors' experience, relatively small flow rates ($\lambda_T < \lambda_{T,fd}$) are usually employed to cool the discs and seal the wheel spaces of gas-turbine engines; blade-cooling flow rates are usually much higher ($\lambda_T > \lambda_{T,fd}$).

Karabay et al. [7] showed that, at sufficiently large values of λ_T, free-vortex flow will occur in the core outside the boundary layers on the rotating surfaces. Under these conditions, $V_{\phi,\infty} \propto r^{-1}$, where $V_{\phi,\infty}$ is the tangential component of velocity in the core. As $V_{\phi,\infty} = \beta_p \Omega r_1$ at the outlet of the pre-swirl nozzles, where $r = r_1$, it follows that, for an ideal system with no losses,

$$\frac{V'_{\phi,\infty}}{\Omega r} = \beta_p x_1^2 x^{-2} \tag{1}$$

for $x \geqslant x_1$, where $x = r/b$ is the nondimensional radius and the dash is used to denote the ideal value.

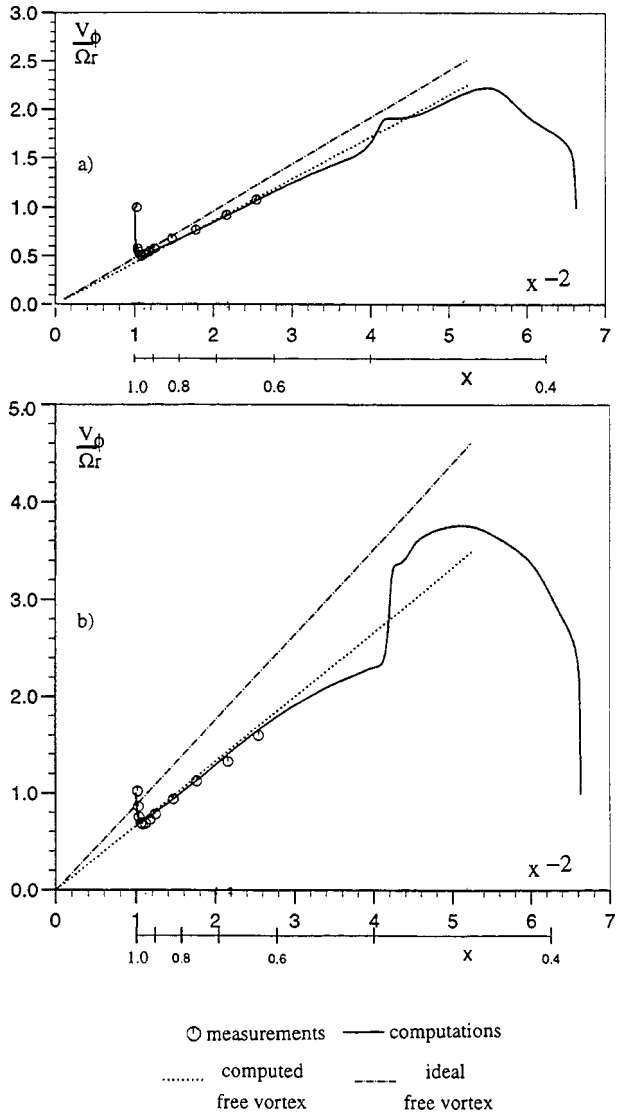

Fig. 5 Comparison between computed and measured variation of $V_\phi/\Omega r$ with x^{-2} for $\lambda_T=0.22$ and $Re_\phi=0.55\times10^6$: (*a*) $\beta_p=2.511$; (*b*) $\beta_p=4.535$.

In the cover-plate system considered here, where $\beta_p>1$, there is a nondimensional radius (x^*, say) at which $V'_{\phi,\infty}=\Omega r^*$. Hence, from Eq. (1),

$$x^*=\beta_p^{1/2}x_1. \tag{2}$$

Karabay et al. [7] showed that, provided $x^*<1$ (that is, $\beta_p x_1^2<1$), free-vortex flow will take place throughout the cavity when

$$\lambda_T \geqslant 0.437[1-(\beta_p x_1^2)^{1.175}]^{1.656}. \tag{3}$$

For smaller values of λ_T, nonentraining Ekman-type layers form in the outer part of the rotating cavity and free-vortex flow is confined to the inner part.

In practical cover-plate systems, there are losses between the outlet of the pre-swirl nozzles and the inlet to the rotating cavity. If $\beta_p>1$, viscous effects cause a loss of angular momentum of the fluid, reducing the effective swirl ratio. It is convenient to introduce an effective pre-swirl ratio, $\beta_{p,\text{eff}}$, where, in comparison with Eq. (1),

$$\frac{V_{\phi,\infty}}{\Omega r}=\beta_{p,\text{eff}}\,x_1^2x^{-2} \tag{4}$$

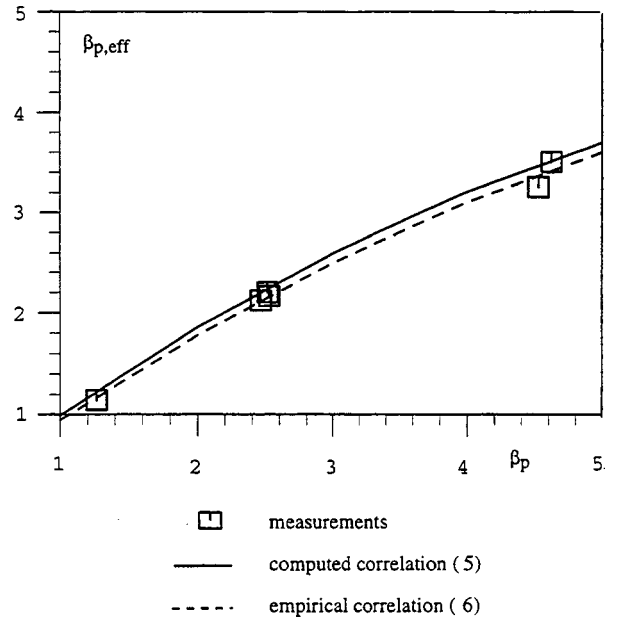

Fig. 6 Variation of $\beta_{p,\text{eff}}$ with β_p for whole system

and, for $\beta_p>1$, $\beta_{p,\text{eff}}<\beta_p$.

This relationship can be shown graphically by plotting $V_{\phi,\infty}/\Omega r$ versus x^{-2}: a free-vortex will appear as a straight line passing through the origin ($x^{-2}=0$); the gradient of this line can be used to calculate $\beta_{p,\text{eff}}$. Figure 5 shows a comparison between the computed and measured variation of $V_{\phi,\infty}/\Omega r$ with x^{-2}. The results were obtained, for $\lambda_T=0.22$ and $Re_\phi=0.55\times10^6$, with $\beta_p=2.511$ and 4.535, using the axisymmetric computational model for the whole system and experimental apparatus described in Section 2. The agreement between the computations and measurements is very good, and there is clear evidence of free-vortex flow. Two straight lines are plotted: the higher one (the ''ideal free vortex'') corresponds to Eq. (1), and the lower one (the ''computed free vortex'') to Eq. (4). For the latter case, the line was arbitrarily forced through the computed value of $V_{\phi,\infty}/\Omega r$ at $x=0.67$ ($x^{-2}=2.22$). It can be seen that the difference between the two lines increases as β_p increases.

Karabay [12] found that the effects of Re_ϕ and λ_T on $\beta_{p,\text{eff}}$ were negligible, and he proposed the following correlation for the computed values of $\beta_{p,\text{eff}}$

$$\frac{\beta_{p,\text{eff}}}{\beta_p}=1.053-0.062\beta_p. \tag{5}$$

A similar correlation was obtained for the experimental measurements where

$$\frac{\beta_{p,\text{eff}}}{\beta_p}=1-0.056\beta_p. \tag{6}$$

The velocity measurements and computations were made over the range: $0.17<\lambda_T<0.35$, $0.5\times10^6<Re_\phi<1.5\times10^6$ and $1.1<\beta_p<4.6$. Figure 6 shows the good agreement between the two correlations and the experimental data, although it should be pointed out that the results were obtained for only one geometry (in which $r_1/b=0.43$).

The fact that $\beta_{p,\text{eff}}<\beta_p$ when $\beta_p>1$ is attributed to the recirculation region, near the inlet to the rotating cavity, in which angular momentum is lost with a consequent reduction in swirl. The fact that the axisymmetric computations agree well with the measurements suggests that the three-dimensional effect of the pre-swirl nozzles is not significant. The losses are strongly related to β_p and only weakly to λ_T or Re_ϕ; the losses may, however,

depend on the system geometry, particularly if the cooling air passes through holes in the cover-plate rather than through an annular slot as considered here.

3.2 Pressure Distribution. Karabay et al. [11] showed that the radial distribution of pressure in the cavity can be estimated from the inviscid one-dimensional radial-momentum equation

$$\frac{1}{\rho}\frac{dp}{dr}=\frac{V_{\phi,\infty}^2}{r}-V_{r,\infty}\frac{dV_{r,\infty}}{dr}, \tag{7}$$

where $V_{\phi,\infty}$ can be approximated by Eq. (4) and $V_{r,\infty}$ from the continuity equation, where

$$V_{r,\infty}=\frac{\dot{m}}{2\pi\rho rs} \tag{8}$$

The local pressure coefficient, C_p, can be defined for compressible flow as

$$C_p=\frac{\gamma}{\gamma-1}\frac{p_1}{\frac{1}{2}\rho_1\Omega^2 r_1^2}\left\{\left(\frac{p}{p_1}\right)^{(\gamma-1)/\gamma}-1\right\}, \tag{9}$$

where, in the limit $p\rightarrow p_1$, the incompressible form is

$$C_p=\frac{p-p_1}{\frac{1}{2}\rho_1\Omega^2 r_1^2}. \tag{10}$$

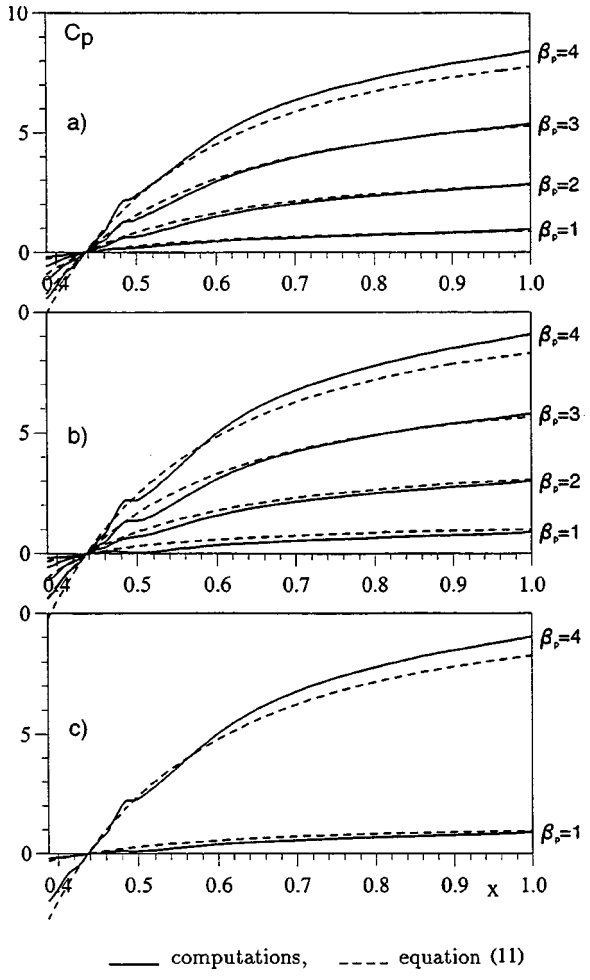

Fig. 7 Radial distribution of computed and theoretical pressure coefficients for whole system: (*a*) $Re_\phi=1.3\times10^6$, $\lambda_T=0.23$; (*b*) $Re_\phi=0.56\times10^6$, $\lambda_T=0.35$; and (*c*) $Re_\phi=1.3\times10^6$, $\lambda_T=0.35$.

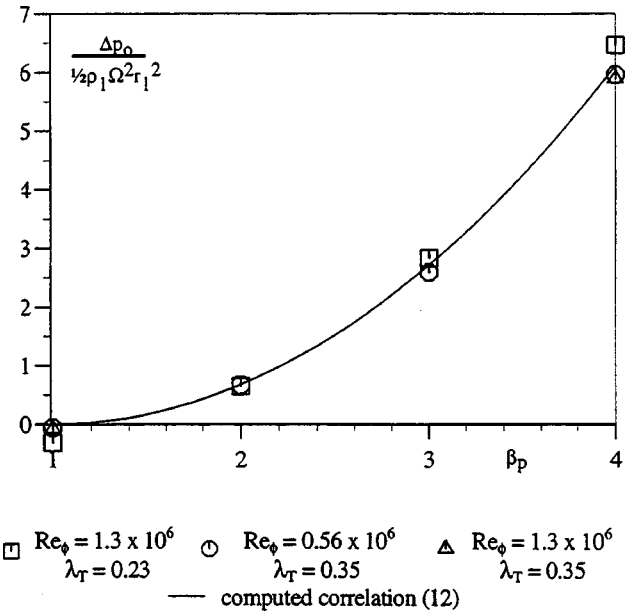

Fig. 8 Computed variation of nondimensional pressure loss β_p for whole system

Equation (7) can be integrated radially from $r=r_1$ to give

$$C_p=\left\{\beta_{p,\text{eff}}^2+\left(\frac{\lambda_T}{2\pi G\,\text{Re}_\phi^{0.2}}\right)^2\left(\frac{b}{r_1}\right)^4\right\}\left\{1-\left(\frac{r_1}{r}\right)^2\right\}. \tag{11}$$

Figure 7 shows comparisons between the computed values of C_p and Eq. (11) for the rig geometry (where $p=p_1$ at $r_1/b=0.43$ and $z/s=0.5$); Eq. (5) was used to calculate $\beta_{p,\text{eff}}$. For $\beta_p\leqslant 3$, the agreement is good; for $\beta_p=4$, Eq. (11) slightly underestimates the computed pressure coefficients. Unfortunately, for the reason given in Section 2.2, no experimental data are available for comparison.

In an engine, the maximum pre-swirl ratio is limited by the available pressure upstream of the pre-swirl nozzles and the necessary pressure at inlet to the blade-cooling passages. The pressure losses in the pre-swirl nozzles and the blade-cooling passages are beyond the scope of this paper. However, the total pressures downstream of the pre-swirl nozzles (at $x=0.43$) and upstream of the blade-cooling passages (at $x=0.97$) were computed at $z/s=0.5$, in a stationary frame of reference, and the difference was used to define the loss in total pressure, Δp_0. This computed loss was correlated for $1<\beta_p<4$ by

$$\frac{\Delta p_0}{\frac{1}{2}\rho_1\Omega^2 r_1^2}=0.678(\beta_p-1)^2. \tag{12}$$

Figure 8 shows a comparison between this correlation and the computations; again there are no experimental data available. In practice, the loss would depend on the system geometry.

4 Thermodynamics and Heat Transfer

4.1 Thermodynamics of Pre-Swirl Process. Karabay et al. [7] used the steady-flow energy equation for an adiabatic pre-swirl system to show that

$$T_{t,2}-T_{0,1}=\frac{\Omega^2 r_2^2}{2c_p}\left(1-2\frac{r_1^2}{r_2^2}\beta_p\right), \tag{13}$$

where $T_{0,1}$ is the total temperature (in a *stationary frame* of reference) of the pre-swirl air (at $r=r_1$) and $T_{t,2}$ is the total temperature (in a *rotating frame*) of the blade-cooling air (at $r=r_2$); it is $T_{t,2}$ that controls the heat transfer inside the blade-cooling pas-

sages. It can be seen from Eq. (13) that $T_{t,2}$ decreases as β_p increases, with beneficial effects for blade cooling.

Karabay et al. [11] extended this adiabatic thermodynamic analysis to the case of a pre-swirl system where heat is transferred from the hot turbine disc to the cooling air; they ignored heat transfer from the cover-plate. Their result can be expressed as

$$T_{t,2}-T_{0,1}=\frac{\Omega^2 r_2^2}{2c_p}\left(1-2\frac{r_1^2}{r_2^2}\beta_p\right)+\pi\left(1-\frac{a^2}{b^2}\right)\times\frac{\mathrm{Nu}_{av}}{\mathrm{Pr}\,C_W}(T_s-T_{s,ad})_{av}. \quad (14)$$

Nu_{av} is the average Nusselt number defined as

$$\mathrm{Nu}_{av}=\frac{q_{s,av}b}{k(T_s-T_{s,ad})_{av}}, \quad (15)$$

and the subscript ''av'' refers to the radially weighted average value; $T_{s,ad}$ is the adiabatic disc-temperature, which is discussed below. Increasing β_p has a beneficial effect in the adiabatic case but what happens when heat transfer is significant? To answer this question, it is useful to use the Reynolds analogy.

4.2 The Reynolds Analogy Applied to Pre-Swirl Systems. Owen and Rogers [9] showed that the Reynolds analogy between angular momentum and heat transfer can be applied to boundary-layer flow in a rotating cavity under certain conditions. The most important of these conditions are that the Prandtl number of the fluid is unity (Pr=1), that the disc-temperature distribution is quadratic ($T_s \propto r^2$) and that the axial distributions of swirl and temperature are similar at entry to the cavity.

For the case of a rotating cavity with free-vortex flow throughout the core (see Section 3.1), Karabay et al. [11] showed that, for the simple rotating cavity, the adiabatic disc-temperature is given by

$$T_{s,ad}=T_{0,1}+\frac{\Omega^2 b^2}{2c_p}[Rx^2-\beta_p x_1^2(1+R)], \quad (16)$$

where R is the recovery factor, which for air can be approximated by $R=\mathrm{Pr}^{1/3}$. They also showed that, when the Reynolds analogy is valid,

$$\mathrm{Nu}_{av}=\frac{\mathrm{Re}_\phi C_m}{\pi\left(1-\frac{a^2}{b^2}\right)\left\{1+\frac{a^2}{b^2}-2\beta_p\frac{r_1^2}{b^2}\right\}}, \quad (17)$$

where C_m is the moment coefficient.

If Nu_{av} is to remain finite then C_m must equal zero when the denominator of Eq. (17) equals zero. This leads to the introduction of the *critical pre-swirl ratio*, $\beta_{p,\mathrm{crit}}$, such that $C_m=0$ when $\beta_p=\beta_{p,\mathrm{crit}}$, where

$$\beta_{p,\mathrm{crit}}=\frac{a^2+b^2}{2r_1^2}. \quad (18)$$

Although this result was derived using the Reynolds analogy, C_m does not depend directly on the Prandtl number of the fluid or on the temperature on the disc. Paradoxically, this implies that Eq. (18) is generally valid for all rotating cavities in which there is free-vortex flow throughout the core regardless of whether or not the Reynolds-analogy conditions are satisfied! Surprisingly, $\beta_{p,\mathrm{crit}}$ depends only on the geometric parameters (a, b, and r_1) and not on the flow parameters (Re_ϕ and λ_T).

Figure 9 shows the computed variation of C_m with β_p for two values of Re_ϕ and λ_T. The computations were carried out using the axisymmetric solver applied to the full pre-swirl system described in Section 2. For C_m, the moment was obtained by integrating the computed tangential component of shear stress from $r=80$ mm to $r=198.9$ mm (which were used for a and b in Eq. (18)); the pre-swirl radius, r_1 was 90 mm. These values give

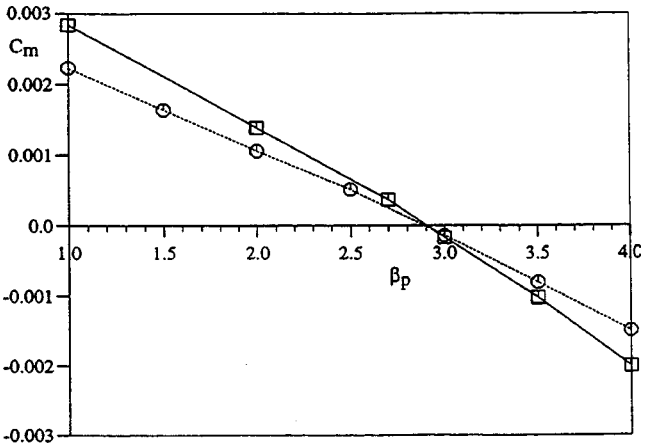

Fig. 9 Computed variation of moment coefficient with β_p for whole system (□ $\mathrm{Re}_\phi=0.56\times10^6$, $\lambda_T=0.35$; ○ $\mathrm{Re}_\phi=1.33\times10^6$, $\lambda_T=0.23$).

$\beta_{p,\mathrm{crit}}=2.837$ according to Eq. (18), and the computed values in Fig. 9 show that $C_m=0$ when $\beta_p=2.9$. For the simple rotating cavity considered by Karabay et al., the difference between the computed and theoretical values of $\beta_{p,\mathrm{crit}}$ were significantly smaller than the 2.2 percent difference found here for the whole system. In view of the complexity of the flow, the agreement between the computed and theoretical values of $\beta_{p,\mathrm{crit}}$ is remarkably good. Although the computations were conducted for only one geometry, there is no reason to believe that Eq. (18) will not be valid for other values of a, b, and r_1.

4.3 Average Nusselt Numbers. Karabay et al. [11] showed computationally that, for the simple cavity, $C_m=C_{m,\mathrm{fd}}$ when $\beta_p=0$, where $C_{m,\mathrm{fd}}$ is the free-disc moment coefficient, the value of which depends on Re_ϕ. They also showed that, when the Reynolds-analogy conditions were satisfied, there is *an optimal pre-swirl ratio*, $\beta_{p,\mathrm{opt}}$, where Nu_{av} is a minimum. The computed ratio $\beta_{p,\mathrm{opt}}/\beta_{p,\mathrm{crit}}$ was found to be less than unity for the Reynolds-analogy case; computations carried out at other conditions showed that the ratio depended on the flow parameters and on the distribution of temperature on the heated disc.

Figure 10 shows the variation of the computed values of Nu_{av} with β_p for the whole pre-swirl system described in Section 2. For $\mathrm{Re}_\phi=1.33\times10^6$ and $\lambda_T=0.23$, there is a minimum value of Nu_{av} at $\beta_p\approx2.5$, but the variation of Nu_{av} with β_p is very small. For $\mathrm{Re}_\phi=1.37\times10^6$ and $\lambda_T=0.35$, the minimum again occurs at $\beta_p\approx2.5$, but for this larger value of λ_T the variation of Nu_{av} is more pronounced. This is consistent with the computations of Karabay et al. for the simple cavity where the variation of Nu_{av} with β_p was found to increase as Re_ϕ and λ_T increased.

The magnitude of Nu_{av} has a direct effect on the temperature of the blade-cooling air, as Eq. (14) shows. The first term on the RHS of Eq. (14) is the adiabatic work term, which decreases as β_p increases; the second is the heat transfer term, which depends on Nu_{av}. For $\beta_p<\beta_{p,\mathrm{opt}}$, the work and heat transfer terms are aligned: $T_{t,2}$ decreases as β_p increases. For $\beta_p>\beta_{p,\mathrm{opt}}$, the two terms are opposed: whether $T_{t,2}$ increases or decreases as β_p increases depends on the relative magnitude of the terms.

The above computations were made with the axisymmetric solver. In the experimental rig, and in a gas turbine, the flow and heat transfer are three-dimensional in the vicinity of the blade-cooling holes. This has a significant effect on the temperature of the blade-cooling air, as discussed below.

4.4 Temperature Rise of Blade-Cooling Air. Karabay [12] used the axisymmetric solver described in Section 2 to compute the bulk-average value of ΔT (where $\Delta T=T_{t,2}-T_{0,1}$) for a range of values of Re_ϕ, λ_T, and β_p. The computed values of ΔT

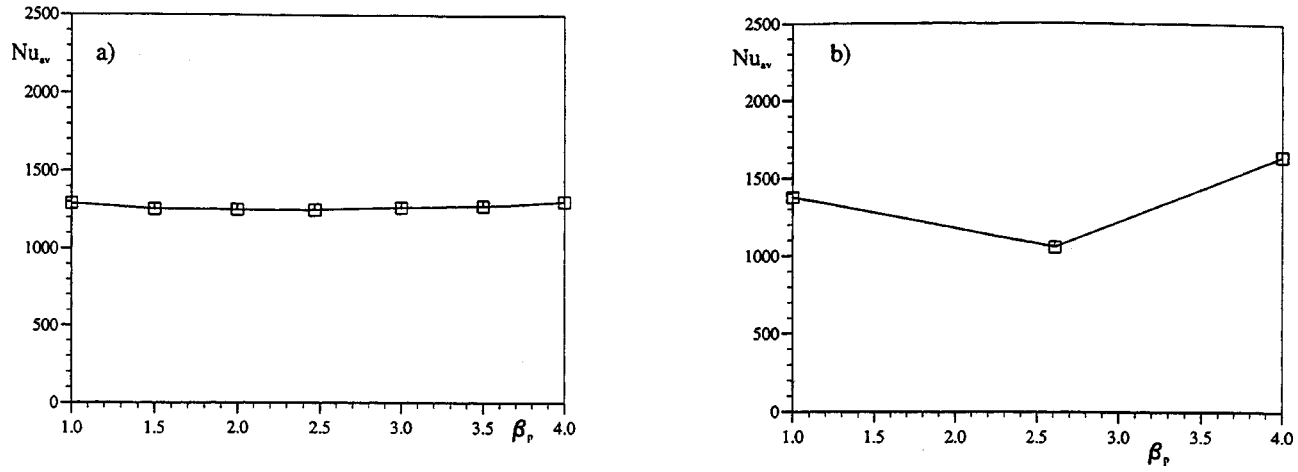

Fig. 10 Computed variation of Nu_{av} with β_p for whole system: (*a*) $Re_\phi=1.33\times10^6$, $\lambda_T=0.23$; (*b*) $Re_\phi=1.37\times10^6$, $\lambda_T=0.35$.

consistently underestimated the measurements: on average, the measured values were 50 percent higher than the computations.

Karabay [12] also describes three-dimensional computations (carried out by Dr. J. X. Chen) of the flow and heat transfer in the simple cavity. These computations were made with a turbulent version (incorporating the Launder-Sharma [13] turbulence model) of the three-dimensional code used by Chen et al. [3,4]. They were conducted for a six-degree segment of the rotating cavity, corresponding to the region around one of the 60 blade-cooling holes in the rotor of the experimental rig. A $65\times60\times11$ (axial×radial×tangential) grid was used, with 72 grid points in the blade-cooling hole. The thermal boundary conditions were similar to those used for the axisymmetric solver, and cyclic symmetry in the tangential direction was assumed on the two radial boundaries.

Figure 11 shows comparisons between computed and measured local Nusselt numbers for five test cases. The two-dimensional computations for the whole system were made using the axisymmetric solver described in Section 2; additional measurements and two-dimensional computations of Nu for the whole system are presented by Pilbrow et al. [8]. The two-dimensional and three-dimensional computations made by Chen were only for the simple cavity, so as to reduce the computational complexity; for the two-dimensional cases, the blade-cooling holes were modeled as an annular equivalent-area slot. Pilbrow et al. [8] produced better agreement between their axisymmetric computations, using the Morse turbulence model, and the measured Nusselt numbers than that shown in Fig. 11, where the Launder-Sharma model was used. Despite the superiority of the Morse model, the Launder-Sharma version was used here for comparison with Chen's computations.

Most of the computed Nusselt numbers shown in Fig. 11 underestimate the measured values. The two-dimensional and three-dimensional computations of Chen, for the simple cavity, are in close agreement over most of the cavity: the largest differences occur in the vicinity of the blade-cooling holes at $x=0.97$. The computations for the simple cavity differ from those for the whole system, particularly at the smaller radii where the computed flows are significantly different.

In the r-ϕ plane, the three-dimensional computations produced very large tangential and radial gradients of both Nusselt numbers and air temperatures near the blade-cooling holes, with the highest temperatures close to the perimeter of the hole and the lowest near the center. Table 1 shows a comparison between the computed and measured values of ΔT for six cases, which were also studied experimentally: $\Delta T(a)$ corresponds to the two-dimensional computations for the whole system, and $\Delta T(b)$ and $\Delta T(c)$ correspond respectively to the two-dimensional and three-dimensional com-

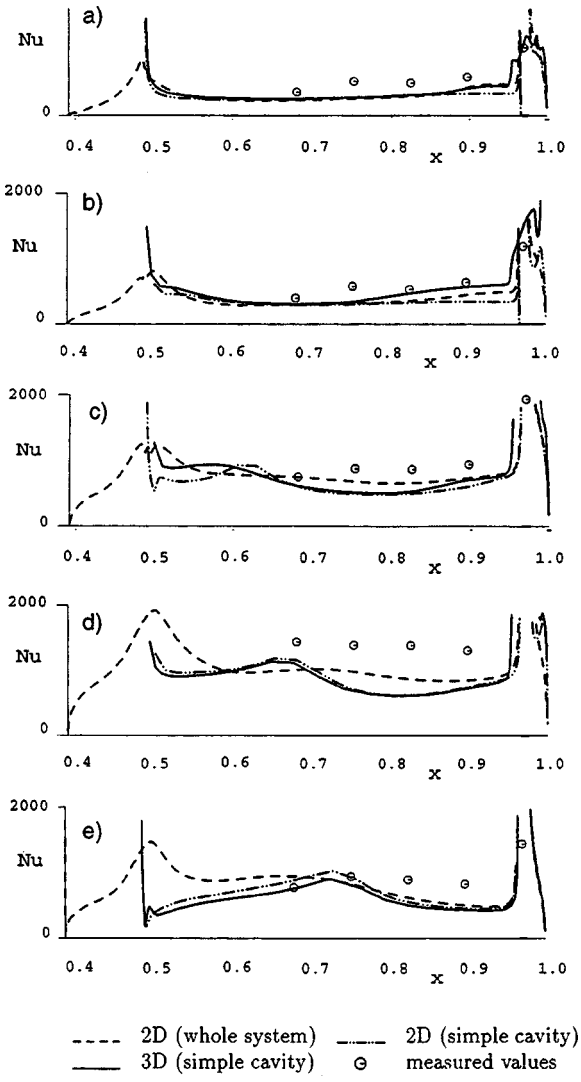

Fig. 11 Comparison between computed and measured radial variation of Nu with x: (*a*) $Re_\phi=0.535\times10^6$, $\lambda_T=0.173$, $\beta_p=1.110$, (*b*) $Re_\phi=0.542\times10^6$, $\lambda_T=0.176$, $\beta_p=1.537$, (*c*) $Re_\phi=0.898\times10^6$, $\lambda_T=0.351$, $\beta_p=2.049$, (*d*) $Re_\phi=0.965\times10^6$, $\lambda_T=0.349$, $\beta_p=2.866$, (*e*) $Re_\phi=0.588\times10^6$, $\lambda_T=0.353$, $\beta_p=3.059$.

Table 1 Comparison between computed and measured values of ΔT(°C): (*a*) two-dimensional, whole system; (*b*) two-dimensional, simple cavity; and (*c*) three-dimensional, simple cavity.

β_p	$Re_\phi \times 10^6$	λ_T	*(a)* ΔT	*(b)* ΔT	*(c)* ΔT	Measured ΔT
1.110	0.535	0.173	12.2	13.2	18.5	21.9
1.267	1.490	0.175	11.9	10.6	15.6	16.2
1.537	0.542	0.176	11.4	11.8	15.1	18.0
2.049	0.898	0.351	6.6	7.3	10.3	10.6
2.866	0.965	0.349	6.2	6.0	7.5	6.5
3.059	0.588	0.353	6.6	7.2	7.9	7.1

putations of Chen for the simple cavity. For most tests, the two-dimensional computations ($\Delta T(a)$ and $\Delta T(b)$) significantly underestimate the measured values, as was noted above, whereas the three-dimensional computations ($\Delta T(c)$) are closer to the measured values. It should be pointed out that, as a consequence of the large velocity and temperature gradients near the blade-cooling holes, the isotropic assumption of the gradient-diffusion modeling of the turbulence is likely to be inaccurate.

In view of the uncertainties in both the computations and the measurements, these results cannot be regarded as conclusive. However, they do strongly suggest that three-dimensional effects have a significant influence on both the heat transfer around the blade-cooling holes and the temperature rise of the cooling air. As discussed in Section 2.2.2, these results underline the need for experimentalists to take great care in how they measure the temperature of the blade-cooling air.

5 Conclusions

A combined theoretical, computational, and experimental study has been undertaken of the flow and heat transfer in a cover-plate pre-swirl system. The results support and extend those presented in earlier studies, and the following conclusions are relevant to the designer of internal cooling-air systems.

- For sufficiently large flow rates, free-vortex flow occurs in the core of fluid outside the boundary layers on the rotating surfaces of the cavity between the cover-plate and the rotor.
- The free-vortex flow is specified by an effective pre-swirl ratio, $\beta_{p,\mathrm{eff}}$, which is smaller than the inlet pre-swirl ratio, β_p, immediately downstream of the pre-swirl nozzles. There is a simple correlation for $\beta_{p,\mathrm{eff}}$, supported by experimental evidence for one particular geometry, and the ratio of $\beta_{p,\mathrm{eff}}/\beta_p$ decreases as β_p increases.
- A theoretical expression for the pressure coefficient, C_p, is in good agreement with computed values for $\beta_p \leqslant 3$. Also, a correlation, based on computed pressures in the system, has been produced relating the loss of total pressure to the pre-swirl ratio. No pressure measurements are available to validate these results.
- It has been shown, theoretically and computationally, that the moment coefficient for the rotor, C_m, decreases as β_p increases. There is a critical pre-swirl ratio, $\beta_{p,\mathrm{crit}}$, for which $C_m = 0$; for $\beta_p > \beta_{p,\mathrm{crit}}$, $C_m < 0$.
- It has been shown computationally that there is an optimal pre-swirl ratio, $\beta_{p,\mathrm{opt}}$, for which the average Nusselt number, Nu_{av}, is a minimum.
- It has been shown theoretically and computationally, using the energy equation, that the total temperature of the blade-cooling air, T_{t2}, depends strongly on β_p: T_{t2} decreases as β_p increases providing $\beta_p < \beta_{p,\mathrm{opt}}$; for $\beta_p > \beta_{p,\mathrm{opt}}$, whether T_{t2} increases or decreases as β_p increases depends on the relative magnitudes of the heat transfer and work terms in the energy equation.
- Computed values of T_{t2} have been compared with experimental measurements. On average, measured increases of air temperature are around 50 percent higher than values obtained with axisymmetric solvers. Three-dimentional computations, giving results much closer to the measured values, show that there are large gradients of air temperature inside the blade-cooling holes. The three-dimentional computations serve to emphasize the need for care in making total-temperature measurements inside blade cooling holes.

In summary, the theoretical expressions for $V_{\phi,\infty}/\Omega r$, C_p, $(T_{t,2} - T_{0,1})$, $(T_{s,ad} - T_{0,1})$, and $\beta_{p,\mathrm{crit}}$ given in Eqs. (4), (11), (14), (16), (18), respectively are expected to apply to other geometries and to other flow parameters as well as to those tested here. However, some quantities, such as the pressure losses and Nusselt numbers, depend strongly on the geometry and on the flow parameters of the individual system. Although this paper has presented a number of concepts and has given theoretical models for some important design parameters, more computational and experimental work is needed to quantify these parameters.

Acknowledgments

The authors thank the UK Engineering and Physical Sciences Research Council and ALSTOM Gas Turbines Ltd. (formerly European Gas Turbines Ltd.) for funding this research project. The three-dimensional computations were conducted by Dr. J. X. Chen while he was at the University of Bath.

Nomenclature

a = inner radius of cavity
b = outer radius of cavity
C_m = moment coefficient ($= M/\frac{1}{2}\rho\Omega^2 b^5$)
C_p = pressure coefficient ($= (p - p_1)/\frac{1}{2}\rho\Omega^2 r_1^2$)
c_p, c_v = specific heat at constant pressure and constant volume, respectively
C_w = nondimensional mass flow rate ($= \dot{m}/\mu b$)
G = gap ratio ($= s/b$)
k = turbulent kinetic energy; thermal conductivity
M = moment for one side of the rotor
$\dot{m}$ = mass flow rate of blade-cooling air
Nu = local Nusselt number $[= rq_s/k(T_s - T_{s,ad})]$
Nu_{av} = average Nusselt number $[= bq_{s,av}/k(T_s - T_{s,ad})_{av}]$
p = static pressure
Pr = Prandtl number ($= \mu c_p/k$)
Pr_t = turbulent Prandtl number
q = heat flux
q_s = convective heat flux from disc to air
r, ϕ, z = radial, tangential and axial coordinates
R = recovery factor
Re_ϕ = rotational Reynolds number ($= \rho\Omega b^2/\mu$)
s = axial width of rotating cavity
S = axial width of whole system
T = temperature
U_τ = friction velocity ($= \sqrt{\tau_w/\rho}$)
V_r, V_ϕ, V_z = time-averaged radial, circumferential, axial components of velocity in a stationary frame
V'_ϕ = ideal value of V_ϕ in a free vortex
x = nondimensional radial coordinate ($= r/b$)
y = distance normal to the wall
y^+ = nondimensional distance ($= \rho y U_\tau/\mu$)
z = axial distance
β_p = pre-swirl ratio ($= V_\phi/\Omega r$ at $r = r_1$)
Δp_0 = loss in total pressure from pre-swirl nozzles to blade-cooling passages
ΔT = total-temperature difference ($= T_{t,2} - T_{0,1}$)
ε = turbulent energy dissipation rate
γ = ratio of specific heats ($= c_p/c_v$)
λ_T = turbulent flow parameter ($= C_w/\mathrm{Re}_\phi^{0.8}$)
μ, μ_t = dynamic and turbulent viscosities
ρ = density
Ω = angular speed of rotor

Subscripts

- ad = adiabatic value
- av = radially-weighted average
- b = blade-cooling air
- crit = value of β_p when $C_m = 0$
- eff = effective value (of β_p)
- fd = free-disc value
- o = total value in stationary frame of reference
- opt = value of β_p when Nu_{av} is minimum
- p = pre-swirl air
- s = disc surface
- t = total value in rotating frame of reference
- ∞ = value in core outside boundary layers
- 1 = inlet to system (at radial location of pre-swirl nozzles)
- 2 = outlet from system (at radial location of blade-cooling holes)

Superscripts

- * = value at stagnation point (where $V_{\phi,\infty} = \Omega r$)

References

[1] Meierhofer, B., and Franklin, C. J., 1981, ''An Investigation of a Pre-swirled Cooling Airflow to a Gas Turbine Disk by Measuring the Air Temperature in the Rotating Channels,'' ASME Paper 81-GT-132.

[2] El-Oun, Z., and Owen, J. M., 1989, ''Pre-Swirl Blade-Cooling Effectiveness in an Adiabatic Rotor-Stator System,'' ASME J. Turbomach., **111**, pp. 522–529.

[3] Chen, J., Owen, J. M., and Wilson, M., 1993, ''Parallel-Computing Techniques Applied to Rotor-Stator Systems: Fluid Dynamics Computations'' in *Numerical Methods in Laminar and Turbulent Flow*, **8**, Pineridge Press, Swansea, pp. 899–911.

[4] Chen, J., Owen, J. M., and Wilson, M., 1993, Parallel-Computing Techniques Applied to Rotor-Stator Systems: Thermal Computations, in *Numerical Methods in Thermal Problems*, **8**, Pineridge Press, Swansea, pp. 1212–1226.

[5] Popp, O., Zimmermann, H., and Kutz, J., 1996, ''CFD Analysis of Cover-Plate Receiver Flow,'' ASME Paper 96-GT-357.

[6] Wilson, M., Pilbrow, R., and Owen, J. M., 1997, ''Flow and Heat Transfer in a Pre-Swirl Rotor-Stator System,'' ASME J. Turbomach., **119**, pp. 364–373.

[7] Karabay, H., Chen, J. X., Pilbrow, R., Wilson, M., and Owen, J. M., 1999, ''Flow in a Cover-Plate Pre-Swirl Rotor-Stator System,'' ASME J. Turbomach., **121**, pp. 160–166.

[8] Pilbrow, R., Karabay, H., Wilson, M., and Owen, J. M., 1999, ''Heat Transfer in a 'Cover-Plate' Pre-Swirl Rotating-Disc System,'' ASME J. Turbomach., **121**, pp. 249–256.

[9] Owen, J. M., and Rogers, R. H., 1989, *Flow and Heat Transfer in Rotating Disc Systems: Vol. 1, Rotor-Stator Systems*, Research Studies Press, Taunton, UK (John Wiley, New York).

[10] Owen, J. M., and Rogers, R. H., 1995, *Flow and Heat Transfer in Rotating Disc Systems: Vol. 2, Rotating Cavities*, Research Studies Press, Taunton, UK (John Wiley, New York).

[11] Karabay, H., Wilson, M., and Owen, J. M., 1999, ''Predicting Effects of Swirl on Flow and Heat Transfer in a Rotating Cavity,'' submitted to Int. J. Heat Fluid Flow.

[12] Karabay, H., 1998, ''Flow and Heat Transfer in a Cover-Plate Pre-Swirl Rotating-Disc System,'' Ph.D. thesis, University of Bath, UK.

[13] Launder, B. E., and Sharma, B. I., 1974, ''Application of the Energy Dissipation Model of Turbulence to the Calculation of the Flow Near a Spinning Disc,'' Letters in *Heat and Mass Transfer*, pp. 131–138.

[14] Morse, A. P., 1988, ''Numerical Prediction of Turbulent Flow in Rotating Cavities,'' ASME J. Turbomach., **110**, pp. 202–215.

[15] Chen, J., Gan, X., and Owen, J. M., 1996, ''Heat Transfer in An Air-Cooled Rotor-Stator System,'' ASME J. Turbomach., **118**, pp. 444–451.